Hindawi Publishing Corporation
International Journal of Photoenergy
Volume 2012, Article ID 472958, 7 pages
doi:10.1155/2012/472958

*Research Article*

# Effects of Calcination Temperatures on Photocatalytic Activity of Ordered Titanate Nanoribbon/$SnO_2$ Films Fabricated during an EPD Process

**Li Zhao,[1,2] Jingrun Ran,[1] Zhan Shu,[1] Guotian Dai,[2] Pengcheng Zhai,[1] and Shimin Wang[2]**

[1] *State Key Laboratory of Advanced Technology for Materials Synthesis and Processing, Wuhan University of Technology, Luoshi Road 122#, Wuhan 430070, China*
[2] *Ministry of Education Key Laboratory for the Green Preparation and Application of Functional Materials, Hubei University, Wuhan 430062, China*

Correspondence should be addressed to Shimin Wang, shiminwang@126.com

Received 13 May 2011; Accepted 15 June 2011

Academic Editor: Jiaguo Yu



Ordered titanate nanoribbon (TNR)/$SnO_2$ films were fabricated by electrophoretic deposition (EPD) process using hydrothermally prepared titanate nanoribbon as a precursor. The formation mechanism of ordered TNR film on the fluorine-doped $SnO_2$ coated (FTO) glass was investigated by scanning electron microscopy (SEM). The effects of calcination temperatures on the phase structure and photocatalytic activity of ordered TNR/$SnO_2$ films were investigated and discussed. The X-ray diffraction (XRD) results indicate that the phase transformation of titanate to anatase occurs at 400°C and with increasing calcination temperature, the crystallization of anatase increases. At 600°C, the nanoribbon morphology still hold and the $TiO_2$/$SnO_2$ film exhibits the highest photocatalytic activity due to the good crystallization, unique morphology, and efficient photogenerated charge carriers separation and transfer at the interface of $TiO_2$ and $SnO_2$.

## 1. Introduction

A large number of investigations have focused on the semiconductor photocatalyst for its applications in solar energy conversion and environmental purification since Fujishima and Honda discovered the photocatalytic splitting of water on the $TiO_2$ electrodes in 1972 [1–9]. Among various oxide semiconductor photocatalysts, titania is a very important photocatalyst for its strong oxidizing power, nontoxicity, and long-term photostability [10–13]. However, $TiO_2$ acting as a photocatalyst has an inherent and significant shortcoming: the fast recombination of the photogenerated charge carriers (hole-electron pairs). Thus, it is of great importance to reduce the recombination of photogenerated charge carriers in $TiO_2$ to enhance its photocatalytic activity for practical and commercial use. Coupling $TiO_2$ with other semiconductors can provide a beneficial solution for this drawback [14–20]. For example, Tada et al. [14, 16, 17] and our previous work [19] conducted a systematic research on the $SnO_2$ as a coupled semiconductor and confirmed that the photogenerated electrons in the $TiO_2$/$SnO_2$ system can accumulate on the $SnO_2$ and photogenerated holes can accumulate on the $TiO_2$ because of the formation of heterojunction at the $TiO_2$/$SnO_2$ interface, which can result in lower recombination rate of photogenerated charge carriers and higher quantum efficiency and thus better photocatalytic activity. Moreover, conventional powder photocatalysts have serious drawbacks such as the need for posttreatment separation in a slurry system and their easy aggregation, resulting in the low photocatalytic activity [14]. Therefore, the development of two-dimensional (2D) film photocatalysts with efficient electron-hole utilization and favorable recycling characteristics is a challenge for practical applications [21].

Various approaches, such as vacuum evaporation, sputtering, chemical vapor deposition, and sol-gel methods, have been contributed to the fabrication of 2D thin film. However, these approaches have some disadvantages for industry applications. Vacuum evaporation, sputtering, and chemical

vapor deposition methods require special apparatuses for deposition of films, and sol-gel method needs coating repeatedly in order to get thick films. Recently, a versatile and facile method, electrophoretic deposition (EPD) method, was successfully utilized to fabricate thin film materials [19, 20]. The EPD method exhibits many advantages, such as higher deposition rate, reproducibility, and efficient control over thickness and morphology of the films through tuning the applied current or potential. Moreover, the EPD method can be used to deposit films on different shaped and sized substrates, which can be extended to a large scale and commercial applications.

Our recent work indicates that titanate nanotube films could be obtained by the EPD method [20]. However, there is no report on the preparation of ordered titanate nanoribbon/$SnO_2$ films for photocatalytic application. Herein, we present a facile and effective approach for the preparation of ordered titanate nanoribbons/$SnO_2$ films by the EPD process using hydrothermally prepared titanate nanoribbon as a precursor. The formation mechanism of ordered titanate nanoribbons films during the EPD process was investigated by SEM results. Moreover, the effects of calcination temperatures on the phase structure and photocatalytic activity of ordered TNR/$SnO_2$ were investigated and discussed.

## 2. Experimental

*2.1. Preparation of Titanate Nanoribbon.* Titanate nanoribbon was synthesized by a hydrothermal method using commercial $TiO_2$ powder (P25, Degussa, Germany) as a starting material according to our previous reported method [22]. In a typical preparation, 1.5 g P25 was mixed with 140 mL of 10 M NaOH solution followed by hydrothermal treatment of the mixture at 200°C in a 200 mL Teflon-lined autoclave for 48 h. After hydrothermal reaction, the precipitate was separated by filtration and washed with a 0.1 M HCl solution and distilled water until the pH value of the rinsing solution reached ca. 6.5, approaching the pH value of the distilled water. The washed sample was dried in a vacuum oven at 60°C for 8 h.

*2.2. Preparation of Ordered TNR/$SnO_2$ Films.* The ordered TNR films were deposited on FTO glass (Sheet resistance 14–20 ohm/sq) using an EPD method. The electrolyte solution was obtained by adding 1.5 g titanate nanoribbons powder to 200 mL mixed solution of 60 mL ethanol and 140 mL distilled water and then ultrasonicated for 20 min. The pH value of the electrolyte was adjusted to about 9.0 by addition of tetra-methyl-ammonium hydroxide for controlling the surface charge of TNR. The isoelectric point of TNR was reported to be about 5.5 [23, 24]. Therefore, TNR in the pH 9 electrolyte solution had a negatively surface charge density and would be attracted to positive electrode. During the EPD, the cleaned FTO glass was kept at a positive potential while pure silver foil was used as the counter electrode. The linear distance between the two electrodes was about 4 cm. The applied voltage was 15 V. The coated substrates were rinsed with distilled water, dried in air, and calcined at 300, 400, 500, and 600°C in air for 2 h, respectively.

*2.3. Characterization.* X-ray diffraction (XRD) patterns were obtained on a D/MAX-RB X-ray diffractometer (Rigaku, Japan) using Cu Ka irradiation at a scan rate of 0.05° $2\theta\,s^{-1}$ and were used to determine the identity of any phase present. The accelerating voltage and the applied current were 15 kV and 20 mA, respectively. Transmission electron microscopy (TEM) and high-resolution transmission electron microscopy (HRTEM) analyses were conducted with an H-600 STEM/EDX PV9100 microscope, using 200 kV accelerating voltage. Morphology observation was performed on a JSM-6700F field emission scanning electron microscope (FESEM, JEOL, Japan).

*2.4. Measurement of Photocatalytic Activity.* Rhodamine B (RhB), one of the N-containing dyes, which are resistant to biodegradation and direct photolysis, is a popular probe molecule in the heterogeneous photocatalysis reaction. It is often used as a tracer dye within water to determine the rate and direction of flow and transport. Rhodamine dyes fluoresce and can thus be detected easily and inexpensively with instruments called fluorometers. Rhodamine dyes are used extensively in biotechnology applications such as fluorescence microscopy, flow cytometry,and fluorescence correlation spectroscopy. In USA, RhB is suspected to be carcinogenic, and thus products containing it must contain a warning on its label. Therefore, we chose it as a model pollutant compound to evaluate the photocatalytic activity of the as-prepared calcined TNR/$SnO_2$ films [25]. Photocatalytic activity of the calcined TNR/$SnO_2$ films was evaluated and compared by the photocatalytic decolorization of RhB aqueous solution at ambient temperature, as reported in the previous studies [25, 26]. The calcined TNR/$SnO_2$ films were settled in a 20 mL RhB aqueous solution with a concentration of $1.0 \times 10^{-5}$ mol $L^{-1}$ in a dish with a diameter of 9.0 cm. A 15 W 365 nm UV lamp (Cole-Parmer Instrument Co.) was used as a light source. The absorbance of RhB at 554 nm was measured by a UV-Vis spectrophotometer (UV2550, Shimadzu, Japan). According to the Lambert-Beer Law [27, 28], the absorbance ($A$) of RhB is proportional to its concentration ($c$), which generally followed the following equation:

$$A = \varepsilon bc, \tag{1}$$

where $\varepsilon$ is the molar absorption coefficient and $b$ is the thickness of the absorption cell. In our experiment, all the testing parameters were kept constant, so the $\varepsilon$ and $b$ can be considered as a constant. Therefore, the changes of the concentration ($c$) of RhB aqueous solution can be determined by a UV-Vis spectrophotometer. As for the RhB aqueous solution with low concentration, its photocatalytic decolorization is a pseudo-first-order reaction and its kinetics may be expressed as follows [29]:

$$\ln\left(\frac{A_0}{A_t}\right) = kt, \tag{2}$$

where $k$ is the apparent rate constant and $A_0$ and $A_t$ are the initial and reaction absorbance of RhB aqueous solution, respectively.

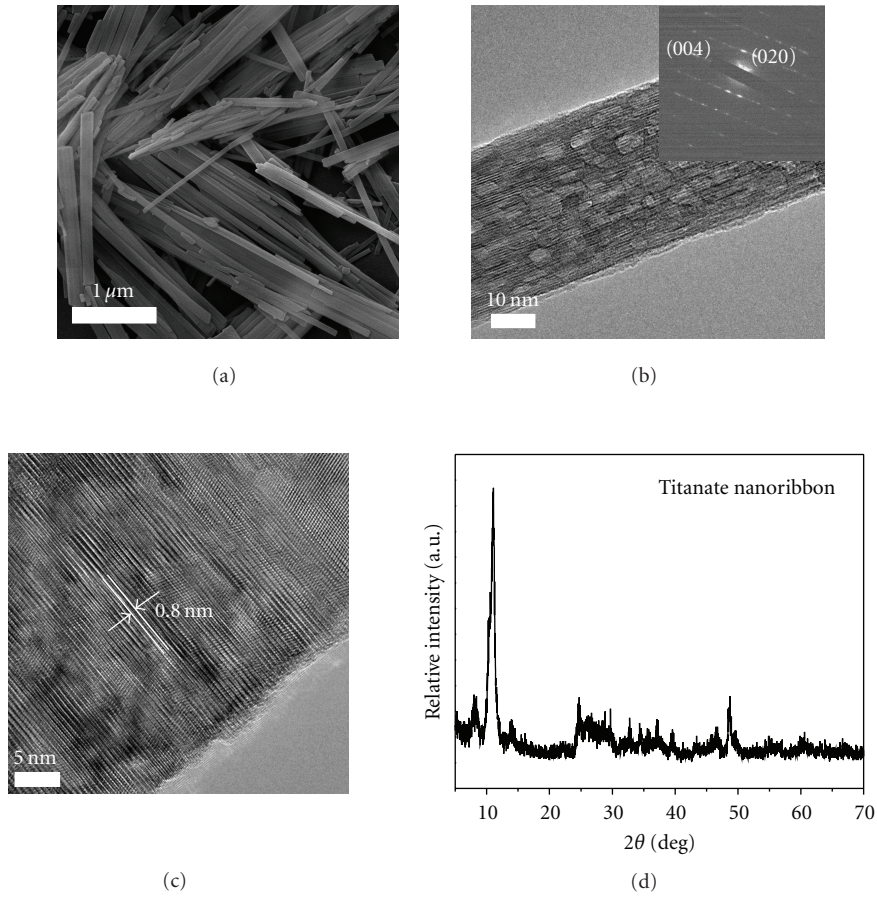


Figure 1: SEM image (a), TEM image (b), SAED pattern (inset in b), HRTEM image (c), and XRD pattern (d) of the as-prepared titanate nanoribbon.

## 3. Results And Discussion

*3.1. Morphology and Phase Structure of the As-Prepared TNR.* Figure 1(a) shows the SEM image of well-dispersed TNR with a length range from several micrometers to several tens of micrometers and a width of 30–300 nm. As shown in Figure 1(b), a typical image of belt-like structure was obtained, indicating a high aspect ratio (the width to the thickness) of 3–15 for the as-prepared TNR, similar to the previous reported work [30]. Moreover, the XRD pattern of as-prepared TNR (Figure 1(d)) exhibited a feature similar to that of alkali or hydrogen titanates such as $H_2Ti_3O_7$ [31], $Na_xH_{2-x}Ti_3O_7$ [32], or $Na_yH_{2-y}Ti_nO_{2n+1}\cdot xH_2O$ [33] due to a similar structure of layered titanate family. TEM and HRTEM were further used to observe the morphology and microstructures of the as-prepared TNR. Figures 1(b) and 1(c) exhibit the TEM and HRTEM images of TNR, respectively. As shown in Figures 1(b) and 1(c), an obvious layered structure in the titanate nanoribbon could be observed, and the layer spacing was about 0.8 nm, corresponding to the diffraction peak located at ca. 11° in Figure 1(b). Moreover, the selected area electron diffraction (SAED) pattern (inset in Figure 1(b)) also reveals that the titanate nanoribbon is single crystalline in structure according to the features of the diffraction pattern.

*3.2. Formation Mechanism of the Ordered TNR Film Deposited on FTO Glass.* The formation mechanism of ordered TNR film is investigated by SEM. As shown in Figure 2(a), before deposition (0 min), FTO glass exhibits relatively rough surfaces, and the $SnO_2$ grains with size of 50–150 nm can be clearly observed. The clear grain boundary indicates that $SnO_2$ is well crystallized. After deposition for 1 min, a large amount of TNRs are randomly deposited on FTO glass (Figure 2(b)). As the deposition time increases, more TNRs are further deposited on the surface of substrate. Interestingly, as the deposition time increased to 3 min, ordered TNR film is obtained (Figure 2(c)). However, why the early formed TNR film appears disorder structure or morphology? This is ascribed to the fact that FTO film contains different sized grains, and thus its surface is not smooth. After deposition for certain time, the surface roughness of FTO film decreases, the electric field near the surface becomes uniform, especially, the negative charged TNRs repel each other, and their strong Brownian motion causes restructure and rearrange of deposited TNR [25].

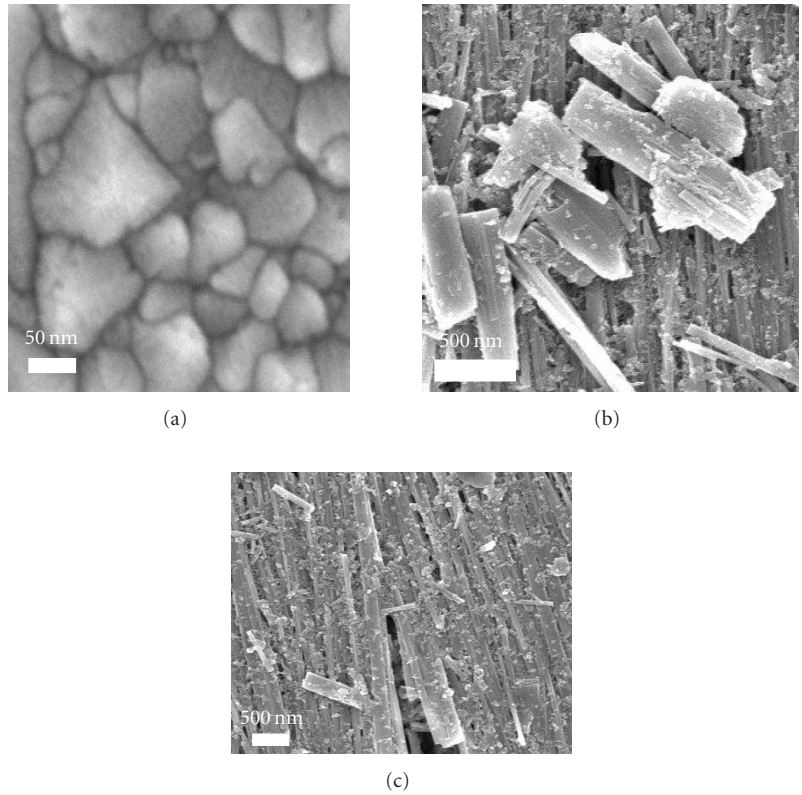


Figure 2: SEM images of FTO glass (a) and TNR films deposited for (b) 1 min and (c) 3 min.

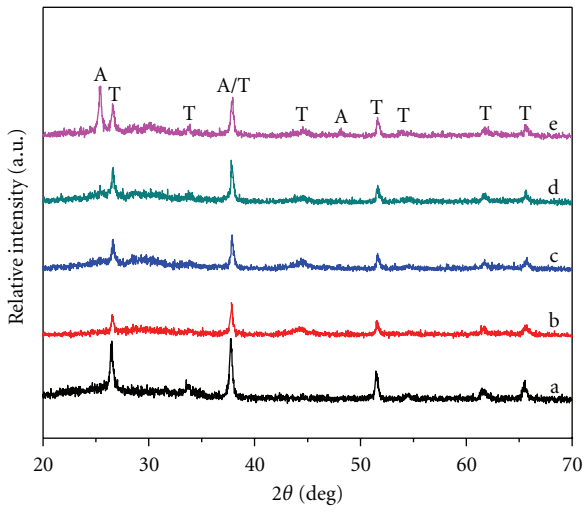


Figure 3: XRD patterns of (a) the substrate and the TNR/$SnO_2$ films calcined at (b) 300, (c) 400, (d) 500, and (e) 600°C.

Therefore, it is not surprising that ordered TNR film can be easily obtained due to the synergistic effects of the above factors [34].

*3.3. Phase Structure and Morphology of the Calcined TNR/$SnO_2$ Film.* XRD was used to identify and determine the phase structures of the calcined TNR/$SnO_2$ film. Figure 3 shows the XRD patterns of the FTO substrate and the TNR/$SnO_2$ film calcined at various temperatures. As shown in Figure 3(a), for pure FTO substrate, strong and sharp diffraction peaks can be observed, and all peaks are indexed to $SnO_2$ (space group: $P4_2/mnm$ (136); $a$ = 4.750 Å, $c$ = 3.198 Å, JCPDS no. 46–1088). Figures 3(b)–3(e) show the XRD patterns of the TNR/$SnO_2$ film calcined at 300 to 600°C. At 300°C, it can be seen that only $SnO_2$ phase is identified in the calcined TNR/$SnO_2$ film and no other diffraction peaks are observed, indicating the amorphous states of TNR film. However, as the calcination temperature increases to 400°C, a small peak at $2\theta$= 25.5° appears, indicating the formation of anatase phase (space group: $I4_1/amd$ (141); $a$ = 3.785 Å, $c$ = 9.514 Å, JCPDS no. 21–1272). With further increase in calcination temperature from 400 to 600°C, the peak intensities of anatase increase, implying the enhancement of crystallization of the anatase phase and the growth of crystallites.

Further observation on the morphology and microstructure of the calcined TNR/$SnO_2$ film was performed with SEM. Figures 4(a) and 4(b) show the surface and cross section SEM images of the TNR/$SnO_2$ film calcined at 600°C for 2 hours. As shown in Figure 4(a), the calcined TNR still exhibits relatively uniform and ordered structure. The nanoribbons are densely packed and deposited almost

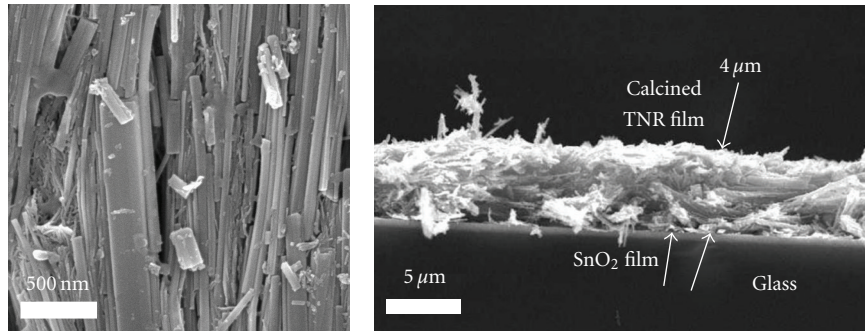


Figure 4: Surface (a) and cross section (b) SEM images of TNR/$SnO_2$ film calcined at 600°C for 2 h.

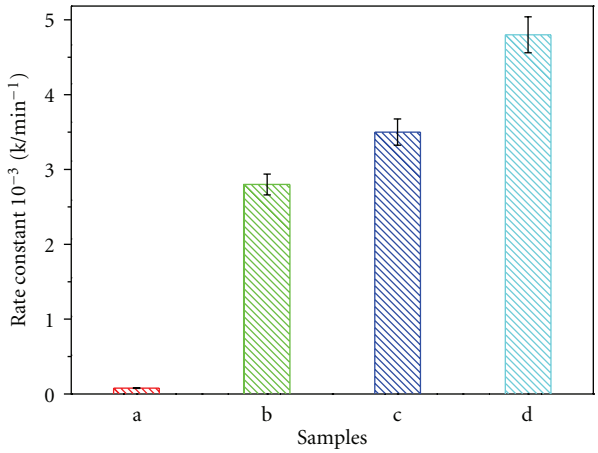


Figure 5: The apparent rate constant ($k$) of TNR/$SnO_2$ films calcined for 2 h at (a) 300, (b) 400, (c) 500, and (d) 600°C.

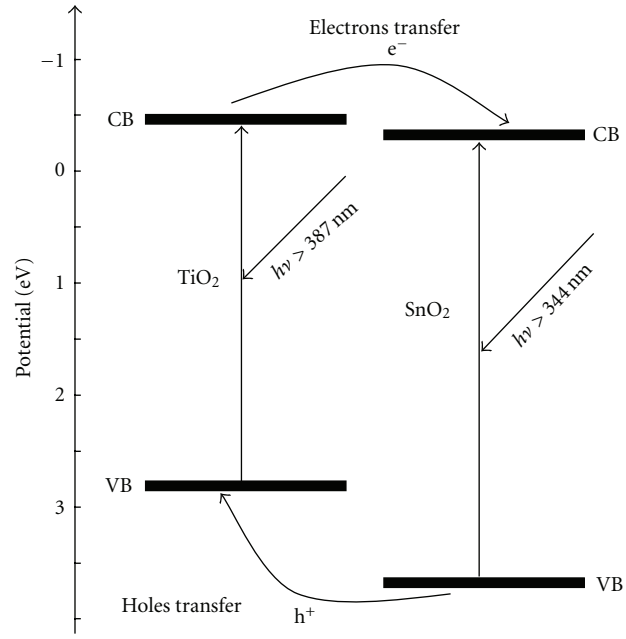


Figure 6: Schematic diagram of the charge-transfer process in the $TiO_2$/$SnO_2$ films.

along the same direction, which are parallel to the substrate, and the thickness of calcined TNR film is about 4 $\mu$m (Figure 4(b)). Moreover, Figure 4(b) shows that the $SnO_2$ film exhibits a thickness of about 500 nm. This SEM observation confirms the intimate contact between $TiO_2$ film and $SnO_2$ film, which could facilitate the interfacial transfer of photogenerated electrons and holes.

*3.4. Photocatalytic Activity of Calcined TNR/$SnO_2$ Films.* The photocatalytic activity of the TNR/$SnO_2$ film calcined at various temperatures was evaluated by photocatalytic decolorization of RhB aqueous solution at room temperature under UV irradiation. However, under dark conditions without light illumination, the concentration of RhB almost does not change for every measurement in the presence of calcined TNR/$SnO_2$ film. Illumination in the absence of calcined TNR/$SnO_2$ film does not result in the photocatalytic decolorization of RhB. Therefore, the presence of both UV illumination and calcined TNR/$SnO_2$ film is necessary for the efficient degradation. Figure 5 shows the apparent rate constants ($k$) of TNR/$SnO_2$ film calcinated at various temperatures. It can be seen that the calcination temperature has a great effect on the photocatalytic activity of the TNR/$SnO_2$ films. The TNR/$SnO_2$ films calcined at 300°C show weak photocatalytic activity probably due to absence or low crystallization of anatase phase in the calcined TNR film. However, when the calcination temperature increases to 400°C, the calcined TNR/$SnO_2$ film shows a decent photocatalytic activity, and the corresponding $k$ value reaches $2.8 \times 10^{-3}$ K/min. This can be attributed to the formation of anatase phase and the bilayer structures of $TiO_2$/$SnO_2$ films in favor of separation of photogenerated charge carrier [14, 16–18, 35–37]. Figure 6 show the charge separation and transfer mechanism of $TiO_2$/$SnO_2$ films. Both $TiO_2$ and $SnO_2$ are $n$-type semiconductors with bandgap energies greater than 3.0 eV and strongly absorb UV light. Upon bandgap excitation, charge carriers (electron-hole pairs) are generated in each semiconductor film. The conduction band (CB) edges of anatase $TiO_2$ and $SnO_2$ are located

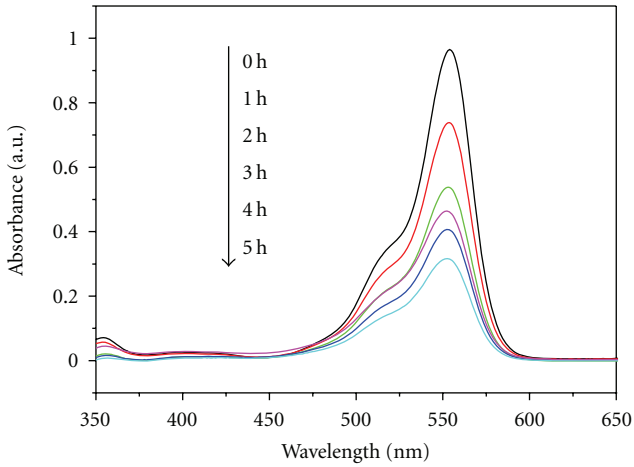


Figure 7: Absorption changes of RhB aqueous solution at room temperature in the presence of the TNR/$SnO_2$ film calcined at 600°C under UV irradiation.

at −0.34 and +0.07 V versus normal hydrogen electrode (NHE) at pH 7, respectively. The valence band (VB) edge of $SnO_2$ (+3.67 V) is more positive than that of anatase $TiO_2$ (+2.87 V) [36, 37]. In terms of the energetics, electrons flow into the $SnO_2$ layer, while holes oppositely diffuse into the $TiO_2$ layer. Consequently, more holes reach the $TiO_2$ surface to cause oxidation reaction, whereas electrons are probably consumed for reduction of $O_2$ at the edge of the $SnO_2$ film. Therefore, the interfacial electrons transfer from $TiO_2$ to $SnO_2$ can explain the high photocatalytic activity of the $TiO_2$/$SnO_2$ films. That is to say, a better charge separation in the composite film is enhanced by a fast electron-transfer process from the conduction band of $TiO_2$ to that of $SnO_2$. Levy et al. [38] and Zhou et al. [19] also reported the same results that photoelectrons and holes transferred toward the reverse direction on the interface of $TiO_2$/$SnO_2$, resulting in a good photocatalytic activity.

As the temperature further increases, the photocatalytic activity of the calcined TNR/$SnO_2$ films increased obviously due to the enhancement of crystallization of anatase (Figure 3). At 600°C, the highest photocatalytic activity is observed, and the $k$ value is about $4.8 \times 10^{-3}$ K/min, which can be ascribed to good crystallization and the fast photogenerated charge carriers separation and transfer at the interface of the calcined TNR/$SnO_2$ films.

Figure 7 shows the change of absorption spectra of RhB aqueous solution during photocatalytic decolorization using the TNR/$SnO_2$ films calcined at 600°C as the photocatalyst. It can be seen that the intensity of absorption peak gradually decreases with increasing UV irradiation time. After UV irradiation for ca. 300 min, the intensity of absorption peak of RhB aqueous solution is very weak, and it becomes colorless, indicating that the calcined TNR films can completely decolorize RhB aqueous solution under UV irradiation. Therefore, the ordered TNR/$SnO_2$ films prepared by the EPD method could be useful for environmental protection such as air purification, water disinfection, and hazardous waste remediation due to their cheap preparation process, controllable structure, strong adhesion, and good photocatalytic activity.

## 4. Conclusions

We have successfully fabricated ordered TNR/$SnO_2$ via an EPD method using hydrothermally prepared TNR as a precursor. The formation mechanism of ordered TNR film on FTO glass substrate was investigated by SEM. The calcination temperature has a great effect on the phase structure and photocatalytic activity of TNR/$SnO_2$ films. When the calcination temperature increases to 600°C, the highest photocatalytic activity was obtained on the calcined TNR/$SnO_2$ film due to the formation of well-crystallized anatase phase, the unique morphology, and the fast charge carrier separation and transfer at the interface of $TiO_2$ and $SnO_2$. This ordered TNR/$SnO_2$ should also have many potential applications in photocatalysis, catalysis, solar cell, and so on.

## Acknowledgments

This work was partially supported by China Postdoctoral Science Foundation funded Project (20100471164). This work was also financially supported by the Hubei Province Key Laboratory of Macromolecular Material, Educational Commission of Hubei Province of China (Q20091007), and Natural Science Foundation of Hubei Province of China (2009CDB351).

## References

[1] A. Fujishima and K. Honda, "Electrochemical photolysis of water at a semiconductor electrode," *Nature*, vol. 238, no. 5358, pp. 37–38, 1972.

[2] M. R. Hoffmann, S. T. Martin, W. Choi, and D. W. Bahnemann, "Environmental applications of semiconductor photocatalysis," *Chemical Reviews*, vol. 95, no. 1, pp. 69–96, 1995.

[3] J. G. Yu and J. R. Ran, "Facile preparation and enhanced photocatalytic $H_2$-production activity of $Cu(OH)_2$ cluster modified $TiO_2$," *Energy & Environmental Science*, vol. 4, no. 4, pp. 1364–1371, 2011.

[4] J. G. Yu, J. F. Xiong, B. Cheng, and S. W. Liu, "Fabrication and characterization of Ag-$TiO_2$ multiphase nanocomposite thin films with enhanced photocatalytic activity," *Applied Catalysis B*, vol. 60, no. 3-4, pp. 211–221, 2005.

[5] F. B. Li, X. Z. Li, and M. F. Hou, "Photocatalytic degradation of 2-mercaptobenzothiazole in aqueous $La^{3+}$-$TiO_2$ suspension for odor control," *Applied Catalysis B*, vol. 48, no. 3, pp. 185–194, 2004.

[6] J. G. Yu, T. T. Ma, and S. W. Liu, "Enhanced photocatalytic activity of mesoporous $TiO_2$ aggregates by embedding carbon nanotubes as electron-transfer channel," *Physical Chemistry Chemical Physics*, vol. 13, no. 8, pp. 3491–3501, 2011.

[7] A. L. Linsebigler, G. Lu, and J. T. Yates, "Photocatalysis on $TiO_2$ surfaces: principles, mechanisms, and selected results," *Chemical Reviews*, vol. 95, no. 3, pp. 735–758, 1995.

[8] P. V. Kamat, R. Huehn, and R. Nicolaescu, "A "sense and shoot" approach for photocatalytic degradation of organic contaminants in water," *Journal of Physical Chemistry B*, vol. 106, no. 4, pp. 788–794, 2002.

[9] J. G. Yu, G. P. Dai, and B. Cheng, "Effect of crystallization methods on morphology and photocatalytic activity of anodized $TiO_2$ nanotube array films," *The Journal of Physical Chemistry C*, vol. 114, no. 45, pp. 19378–19385, 2010.

[10] M. Ni, M. K. H. Leung, D. Y. C. Leung, and K. Sumathy, "A review and recent developments in photocatalytic

water-splitting using $TiO_2$ for hydrogen production," *Renewable and Sustainable Energy Reviews*, vol. 11, no. 3, pp. 401–425, 2007.

[11] Y. X. Li, G. X. Lu, and S. B. Li, "Photocatalytic transformation of rhodamine B and its effect on hydrogen evolution over $Pt/TiO_2$ in the presence of electron donors," *Journal of Photochemistry and Photobiology A*, vol. 152, no. 1–3, pp. 219–228, 2002.

[12] J. G. Yu, Y. R. Su, and B. Cheng, "Template-free fabrication and enhanced photocatalytic activity of hierarchical macro-/mesoporous titania," *Advanced Functional Materials*, vol. 17, no. 12, pp. 1984–1990, 2007.

[13] A. A. Nada, M. H. Barakat, H. A. Hamed, N. R. Mohamed, and T. N. Veziroglu, "Studies on the photocatalytic hydrogen production using suspended modified $TiO_2$ photocatalysts," *International Journal of Hydrogen Energy*, vol. 30, no. 7, pp. 687–691, 2005.

[14] H. Tada, A. Hattori, Y. Tokihisa, K. Imai, N. Tohge, and S. Ito, "A patterned-$TiO_2/SnO_2$ bilayer type photocatalyst," *Journal of Physical Chemistry B*, vol. 104, no. 19, pp. 4585–4587, 2000.

[15] Z. Liu, D. D. Sun, P. Guo, and J. O. Leckie, "An efficient bicomponent $TiO_2/SnO_2$ nanofiber photocatalyst fabricated by electrospinning with a side-by-side dual spinneret method," *Nano Letters*, vol. 7, no. 4, pp. 1081–1085, 2007.

[16] T. Kawahara, Y. Konishi, H. Tada, N. Tohge, and S. Ito, "Patterned $TiO_2/SnO_2$ bilayer type photocatalyst. 2. Efficient dehydrogenation of methanol," *Langmuir*, vol. 17, no. 23, pp. 7442–7445, 2001.

[17] H. Tada, Y. Konishi, A. Kokubu, and S. Ito, "Patterned $TiO_2/SnO_2$ bilayer type photocatalyst. 3. Preferential deposition of Pt particles on the $SnO_2$ underlayer and its effect on photocatalytic activity," *Langmuir*, vol. 20, no. 9, pp. 3816–3819, 2004.

[18] Y. Cao, X. Zhang, W. Yang et al., "A bicomponent $TiO_2/SnO_2$ particulate film for photocatalysis," *Chemistry of Materials*, vol. 12, no. 11, pp. 3445–3448, 2000.

[19] M. H. Zhou, J. G. Yu, S. W. Liu, P. C. Zhai, and L. Jiang, "Effects of calcination temperatures on photocatalytic activity of $SnO_2/TiO_2$ composite films prepared by an EPD method," *Journal of Hazardous Materials*, vol. 154, no. 1–3, pp. 1141–1148, 2008.

[20] J. G. Yu and M. H. Zhou, "Effects of calcination temperature on microstructures and photocatalytic activity of titanate nanotube films prepared by an EPD method," *Nanotechnology*, vol. 19, no. 4, Article ID 045606, 2008.

[21] J. G. Yu, X. J. Zhao, and Q. N. Zhao, "Effect of surface structure on photocatalytic activity of $TiO_2$ thin films prepared by sol-gel method," *Thin Solid Films*, vol. 379, no. 1-2, pp. 7–14, 2000.

[22] H. G. Yu, J. G. Yu, B. Cheng, and M. H. Zhou, "Effects of hydrothermal post-treatment on microstructures and morphology of titanate nanoribbons," *Journal of Solid State Chemistry*, vol. 179, no. 2, pp. 349–354, 2006.

[23] H. Tokudome and M. Miyauchi, "Electrochromism of titanate-based nanotubes," *Angewandte Chemie*, vol. 44, no. 13, pp. 1974–1977, 2005.

[24] H. Tokudome and M. Miyauchi, "Titanate nanotube thin films via alternate layer deposition," *Chemical Communications*, vol. 10, no. 8, pp. 958–959, 2004.

[25] J. G. Yu and L. F. Qi, "Template-free fabrication of hierarchically flower-like tungsten trioxide assemblies with enhanced visible-light-driven photocatalytic activity," *Journal of Hazardous Materials*, vol. 169, no. 1–3, pp. 221–227, 2009.

[26] J. G. Yu, Q. J. Xiang, J. R. Ran, and S. Mann, "One-step hydrothermal fabrication and photocatalytic activity of surface-fluorinated $TiO_2$ hollow microspheres and tabular anatase single micro-crystals with high-energy facets," *CrystEngComm*, vol. 12, no. 3, pp. 872–879, 2010.

[27] H. Kumazawa, M. Inoue, and T. Kasuya, "Photocatalytic degradation of volatile and nonvolatile organic compounds on titanium dioxide particles using fluidized beds," *Industrial and Engineering Chemistry Research*, vol. 42, no. 14, pp. 3237–3244, 2003.

[28] D. Hornero-Mendez and M. I. Minguez-Mosquera, "Rapid spectrophotometric determination of red and yellow isochromic carotenoid fractions in paprika and red pepper oleoresins," *Journal of Agricultural and Food Chemistry*, vol. 49, no. 8, pp. 3584–3588, 2001.

[29] J. G. Yu, H. G. Yu, B. Cheng, X. J. Zhao, J. C. Yu, and W. K. Ho, "The effect of calcination temperature on the surface microstructure and photocatalytic activity of $TiO_2$ thin films prepared by liquid phase deposition," *The Journal of Physical Chemistry B*, vol. 107, no. 50, pp. 13871–13879, 2003.

[30] J. Yu, J. C. Yu, W. Ho, L. Wu, and X. Wang, "A simple and general method for the synthesis of multicomponent $Na_2V_6O_{16}\bullet 3H_2O$ single-crystal nanobelts," *Journal of the American Chemical Society*, vol. 126, no. 11, pp. 3422–3423, 2004.

[31] Q. Chen, W. Z. Zhou, G. H. Du, and L. M. Peng, "Trititanate nanotubes made via a single alkali treatment," *Advanced Materials*, vol. 14, no. 17, pp. 1208–1211, 2002.

[32] X. M. Sun and Y. D. Li, "Synthesis and characterization of ion-exchangeable titanate nanotubes," *Chemistry*, vol. 9, no. 10, pp. 2229–2238, 2003.

[33] J. Canales and P. G. Bruce, "$TiO_2$-B nanowires," *Angewandte Chemie*, vol. 43, no. 17, pp. 2286–2288, 2004.

[34] L. Zhao, J. G. Yu, J. J. Fan, P. C. Zhai, and S. M. Wang, "Dye-sensitized solar cells based on ordered titanate nanotube films fabricated by electrophoretic deposition method," *Electrochemistry Communications*, vol. 11, no. 10, pp. 2052–2055, 2009.

[35] K. Vinodgopal and P. V. Kamat, "Enhanced rates of photocatalytic degradation of an azo dye using $SnO_2/TiO_2$ coupled semiconductor thin films," *Environmental Science and Technology*, vol. 29, no. 3, pp. 841–845, 1995.

[36] J. Shang, W. Yao, Y. Zhu, and N. Wu, "Structure and photocatalytic performances of glass/$SnO_2/TiO_2$ interface composite film," *Applied Catalysis A*, vol. 257, no. 1, pp. 25–32, 2004.

[37] A. Hattori, Y. Tokihisa, H. Tada, and S. Ito, "Acceleration of oxidations and retardation of reductions in photocatalysis of a $TiO_2/SnO_2$ bilayer-type catalyst," *Journal of the Electrochemical Society*, vol. 147, no. 6, pp. 2279–2283, 2000.

[38] B. Levy, W. Liu, and S. Gilbert, "Directed photocurrents in nanostructured $TiO_2/SnO_2$ heterojunction diodes," *Journal of Physical Chemistry B*, vol. 101, no. 10, pp. 1810–1816, 1997.